# Electronic Supplementary information

**a**

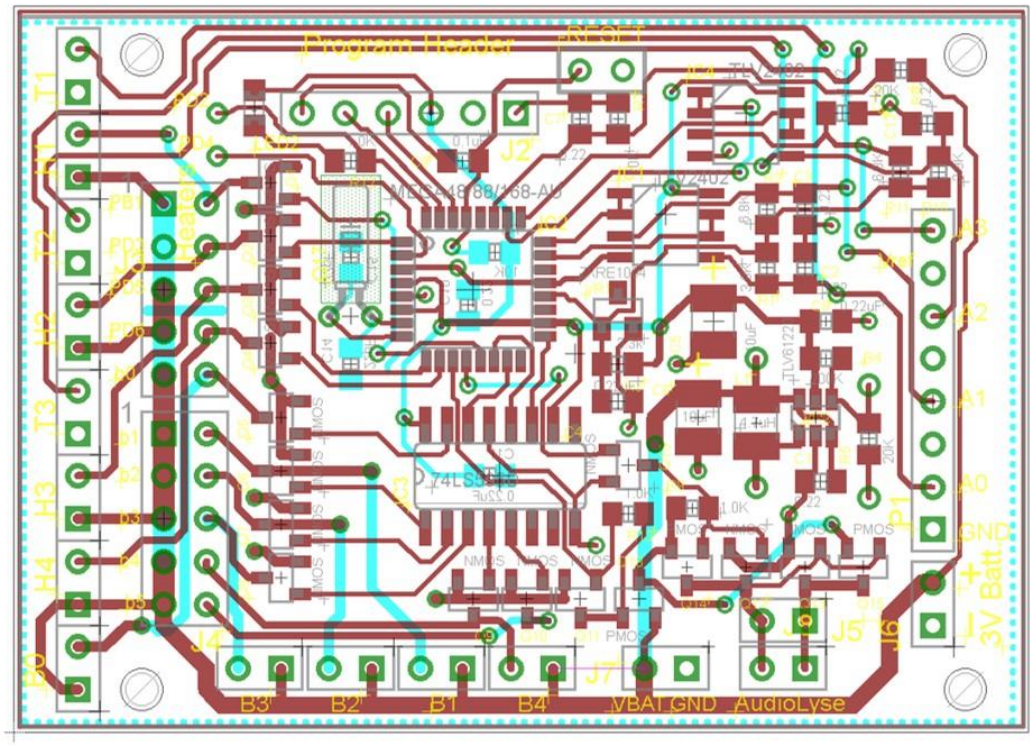


**b**

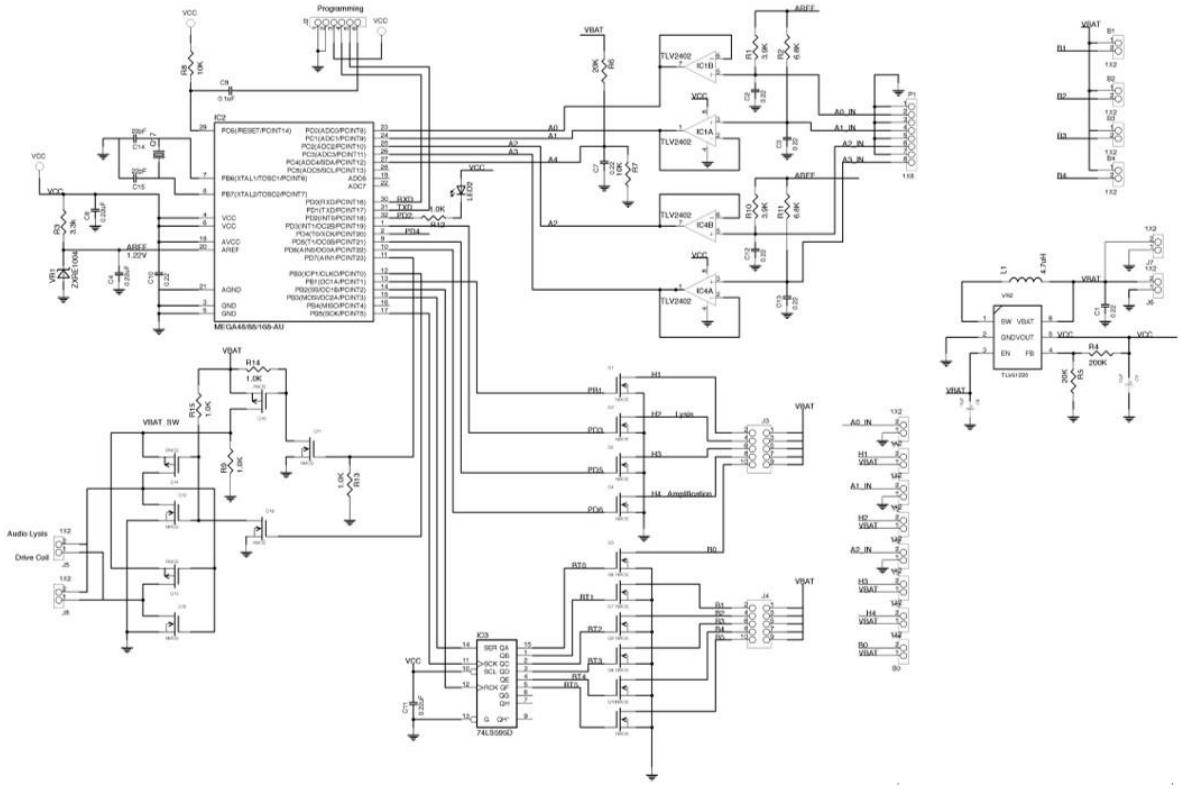


**Fig. S1** Control board design. (**a**) Layout for custom PCB. (**b**) Electronics schematic.

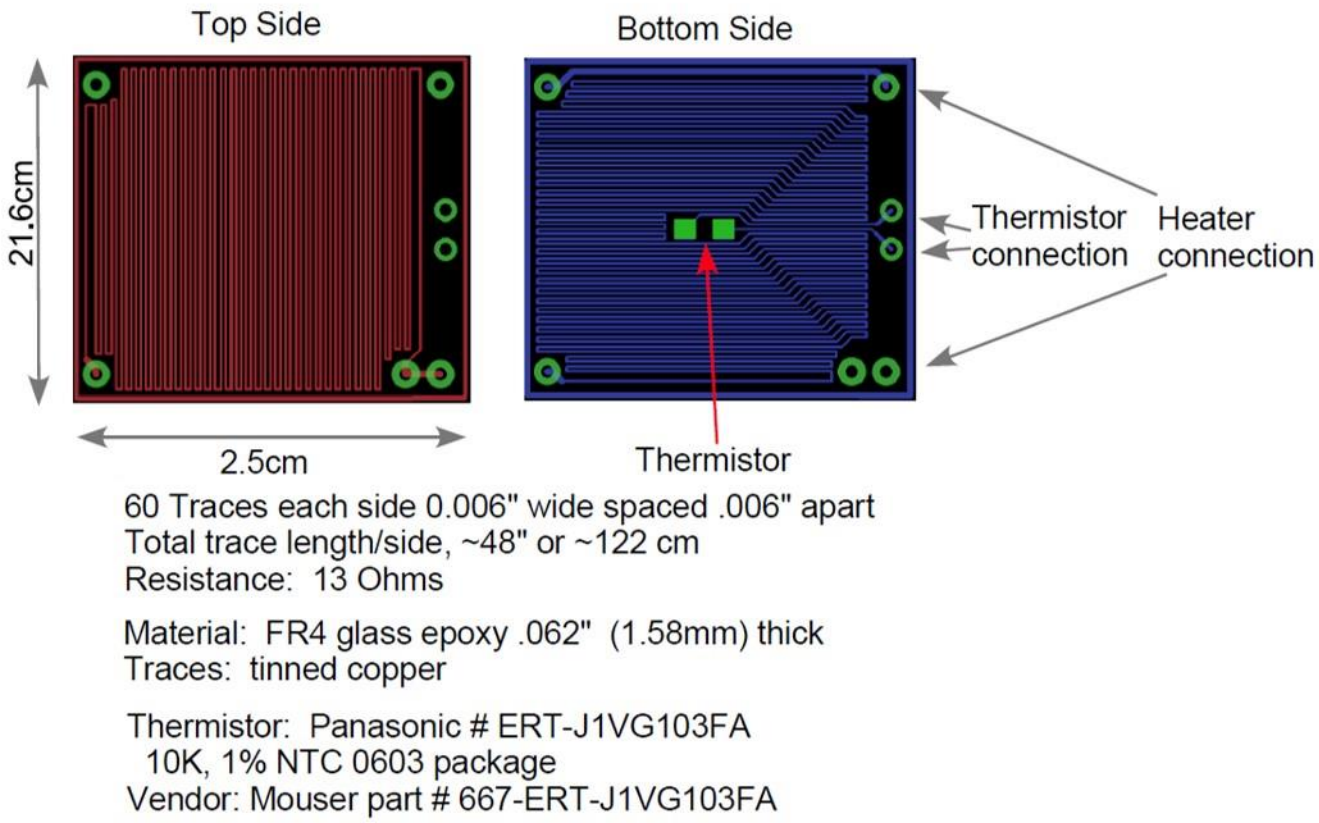


**Fig. S2** Amplification heater design.

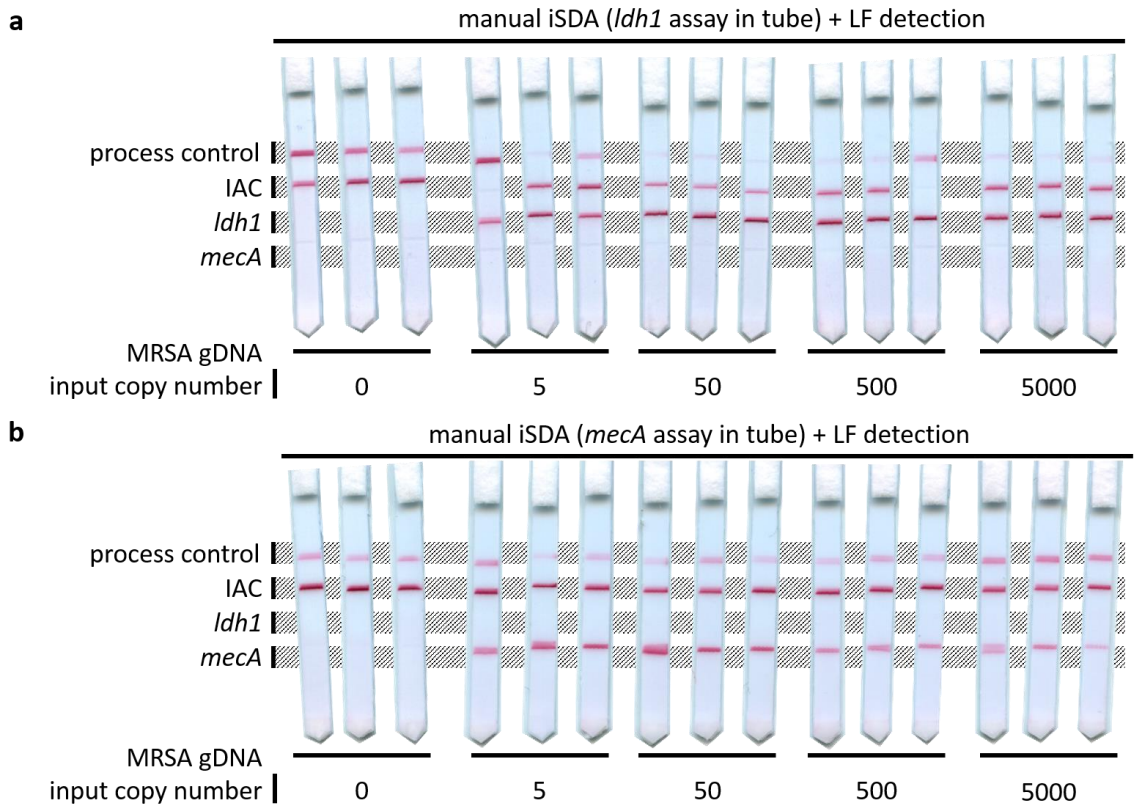


**Fig. S3** Manual iSDA and LF detection result for (**a**) *ldh1* and (**b**) *mecA* assays at low copy numbers of MRSA genomic DNA (gDNA) template. Amplifications were performed in tubes. The results were mixed to salt and Tween-20 to final concentrations of 600 mM and 1% w/v, respectively, then allowed to flow on LF strips. The assay showed robust detection down to at least five copies.

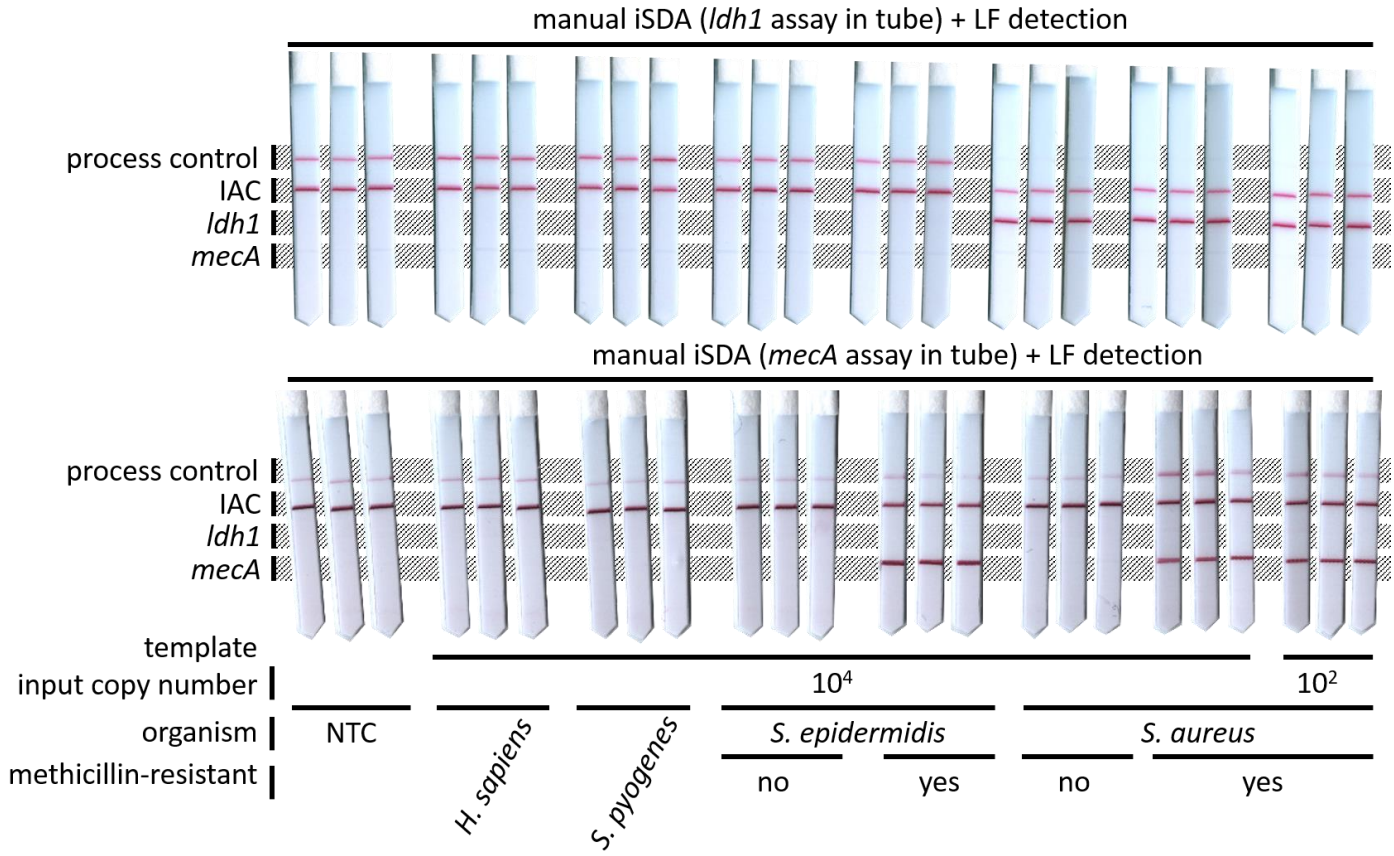


**Fig. S4** Manual iSDA and LF detection result for (**a**) *ldh1* and (**b**) *mecA* assays using no template (NTC); and $10^4$ copies of human, *S. pyogenes*, methicillin-sensitive *S. epidermidis* (MSSE), methicillin-resistant *S. epidermidis* (MRSE), methicillin-sensitive *S. aureus* (MSSA), and methicillin-resistant *S. aureus* (MRSA) gDNA templates (left-to-right). Amplifications were performed in tubes. The results were mixed with salt and Tween-20 in PBS to final concentrations of 600 mM and 1% w/v, respectively, then allowed to flow on LF strips. The strips shown are the last each of a set of two *ldh1* and six *mecA* experiments. The previous experiments showed low-level signal on all nominally negative test lines, including in the NTC condition, and occasional IAC drop-outs in negative tests, which indicated invalid results. These errors were eliminated through use of new stocks of gold nanoparticles and IAC template, respectively. Across the 120 nominally negative conditions tested in the entire set of eight experiments, one NTC and one *S. pyogenes* template yielded a strong false positive, which may be indicative of contamination from five years of running these amplification assays in a single laboratory and open handling of amplicons for lateral flow detection and gel analysis.

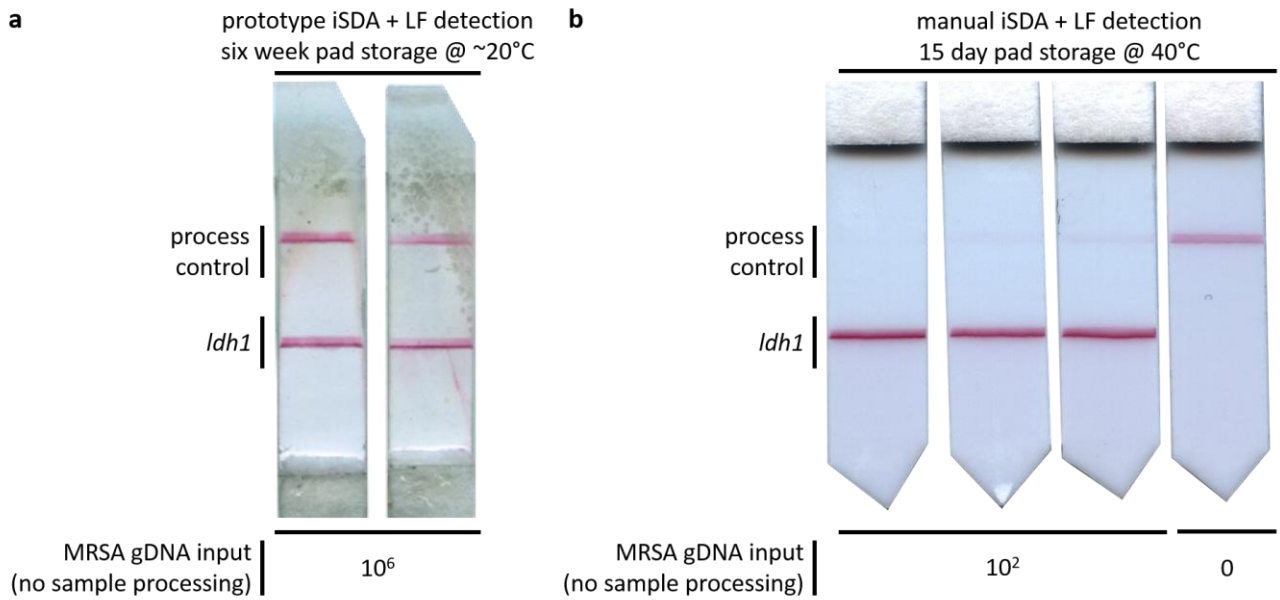


**Fig. S5** Detection results excerpted from dry storage study. (**a**) Prototype iSDA and LF detection on MRSA genomic DNA input using pads stored for six weeks at laboratory ambient temperature in desiccated conditions. Duplicate tests confirm dry reagent viability in these conditions through ldh1 amplification and detection functionality. (**b**) Manual assay tests on low input copy number MRSA genomic DNA using pads stored for 15 days at 40°C in desiccated conditions. Triplicate tests confirm dry reagent viability in these conditions through ldh1 amplification and detection functionality. Associated negative control indicates no contamination.

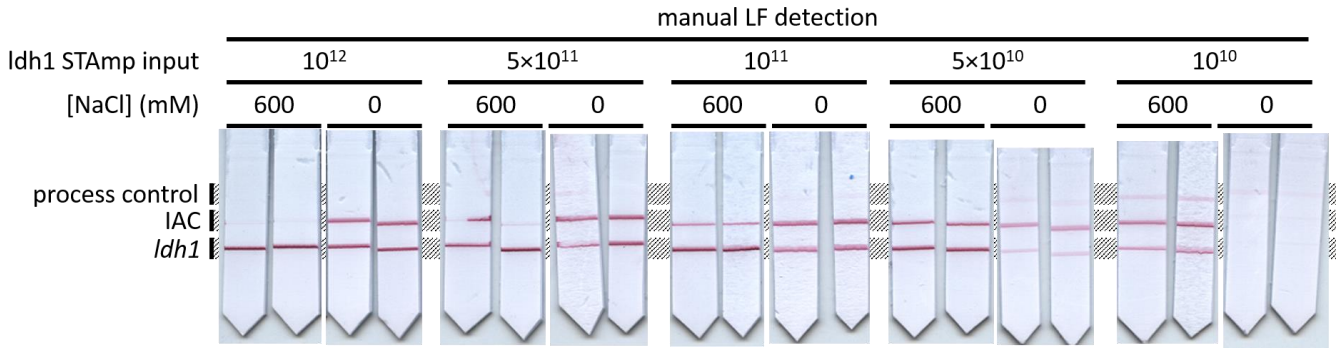


**Fig. S6** Detection results showing impact of salt condition on pDNA binding at ~20°C. A synthetic truncated amplicon (STAmp), which replicated the binding region of the amplicon output by the ldh1 iSDA reaction, was mixed with detection reagents with and without 600 mM NaCl, and allowed to flow on LF strips. Limit of detection was worse in the no-salt condition.

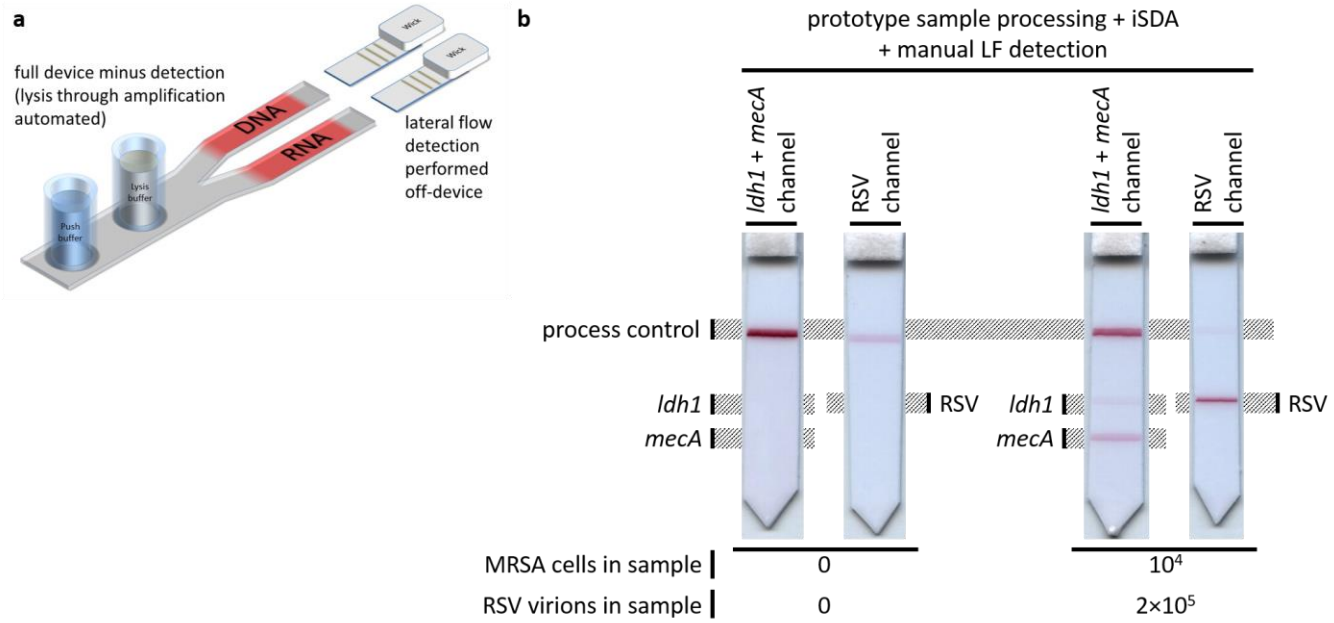


**Fig. S7** DNA and RNA detection in partial prototype test. (**a**) Cartoon of experimental setup. Sample introduction and processing, and amplification were performed on a prototype device. Amplification pads were then removed from the 2DPN and centrifuged at 10,000 ×g for 3 minutes. The resulting fluid was mixed to salt and Tween-20 to final concentrations of 600 mM and 1% w/v, respectively, then allowed to flow on LF strips. (**b**) Results show clean negatives, and positive amplification

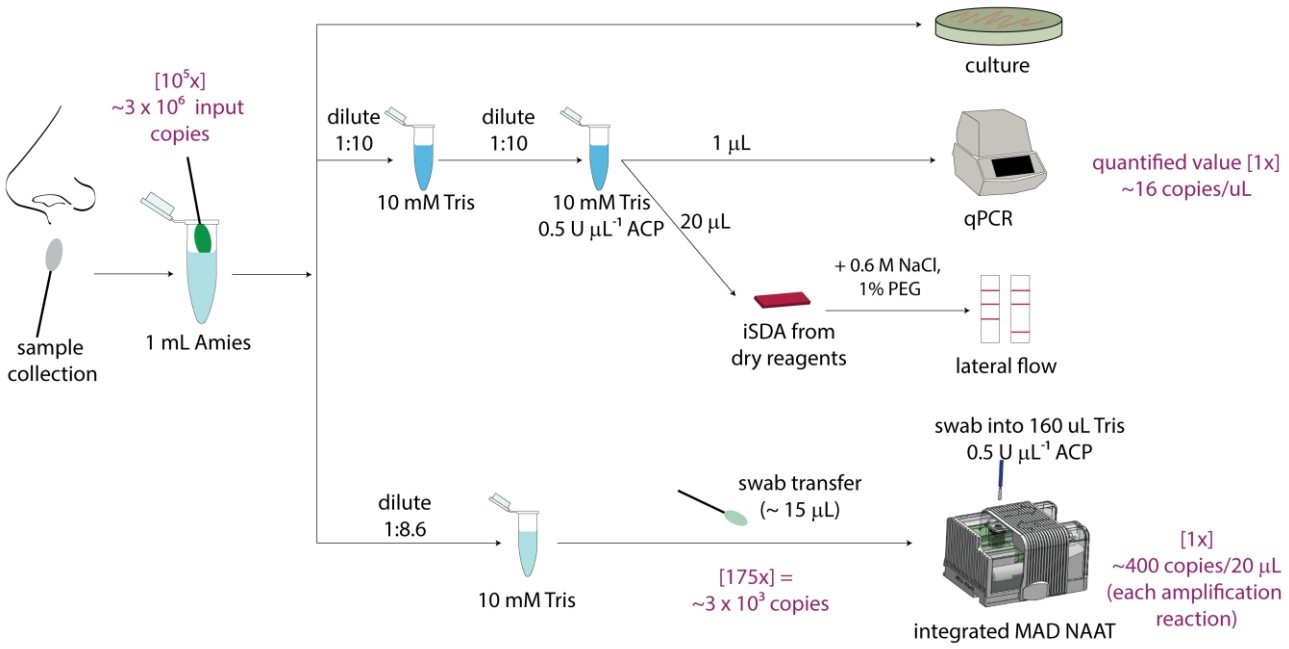


**Fig. S8** Illustration of methods for each patient specimen test. Green text tracks the calculations of estimated copy sensitivity. The ~16 copies $uL^{-1}$ was quantified by qPCR for the lowest input where qPCR found target (PS4, *mecA*) and MAD NAAT showed this sample positive by LF detection. The MAD NAAT prototype held an input volume of 160 µL on-device buffer plus ~15 µL sample, and an amplification zone volume of 20 µL. That corresponded to a minimum detected value of ~$3\times10^3$ input copies in the MAD NAAT prototype.

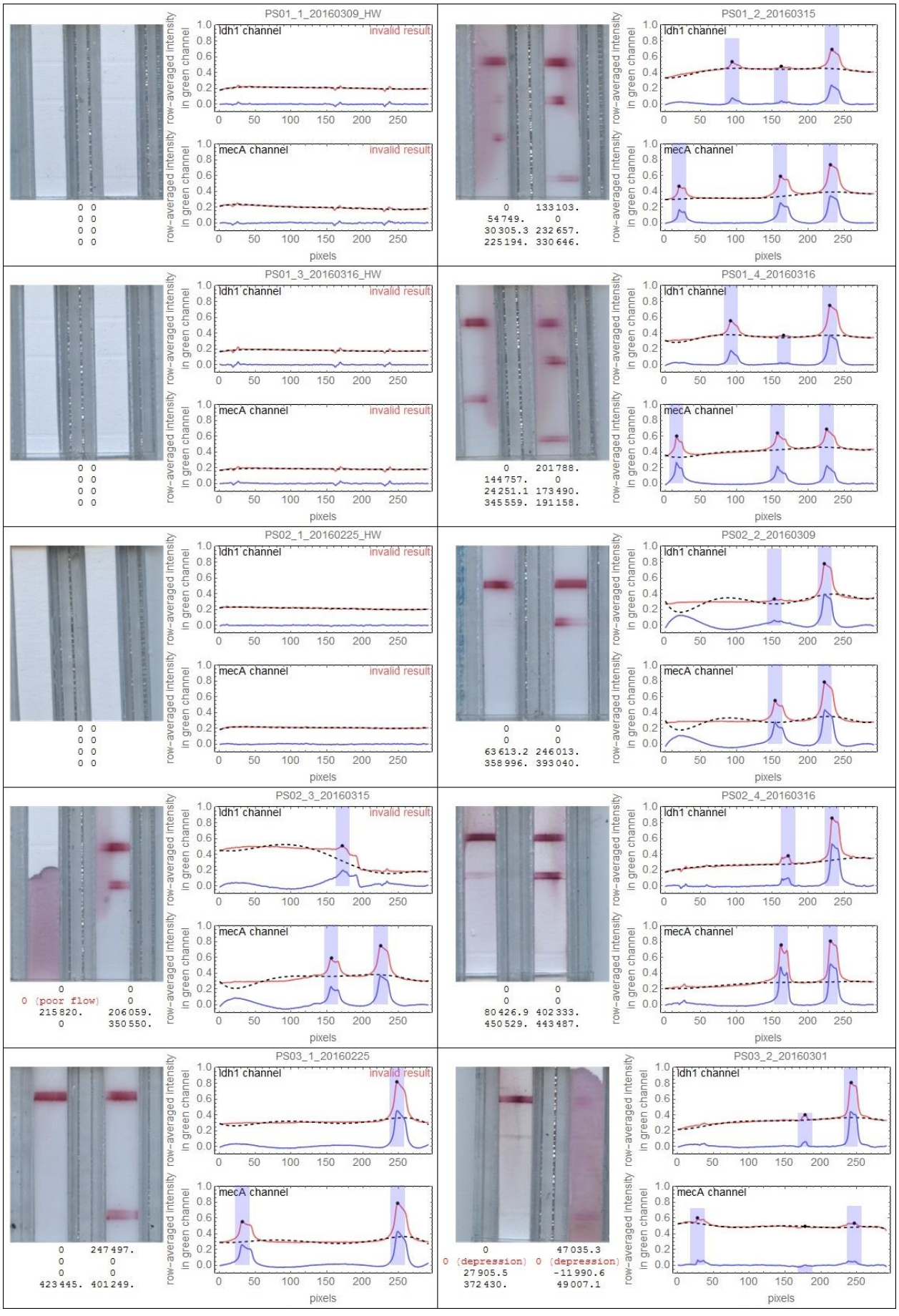
PS01_1_20160309_HW
ldh1 channel
invalid result
mecA channel
invalid result
row-averaged intensity in green channel
pixels
0 0
0 0
0 0
0 0
PS01_2_20160315
ldh1 channel
mecA channel
0 133103.
54749. 0
30305.3 232657.
225194. 330646.
PS01_3_20160316_HW
ldh1 channel
invalid result
mecA channel
invalid result
0 0
0 0
0 0
0 0
PS01_4_20160316
ldh1 channel
mecA channel
0 201788.
144757. 0
24251.1 173490.
345559. 191158.
PS02_1_20160225_HW
ldh1 channel
invalid result
mecA channel
invalid result
0 0
0 0
0 0
0 0
PS02_2_20160309
ldh1 channel
mecA channel
0 0
0 0
63613.2 246013.
358996. 393040.
PS02_3_20160315
ldh1 channel
invalid result
mecA channel
0 0
0 (poor flow) 0
215820. 206059.
0 350550.
PS02_4_20160316
ldh1 channel
mecA channel
0 0
0 0
80426.9 402333.
450529. 443487.
PS03_1_20160225
ldh1 channel
invalid result
mecA channel
0 247497.
0 0
0 0
423445. 401249.
PS03_2_20160301
ldh1 channel
mecA channel
0 47035.3
0 (depression) 0 (depression)
27905.5 -11990.6
372430. 49007.1

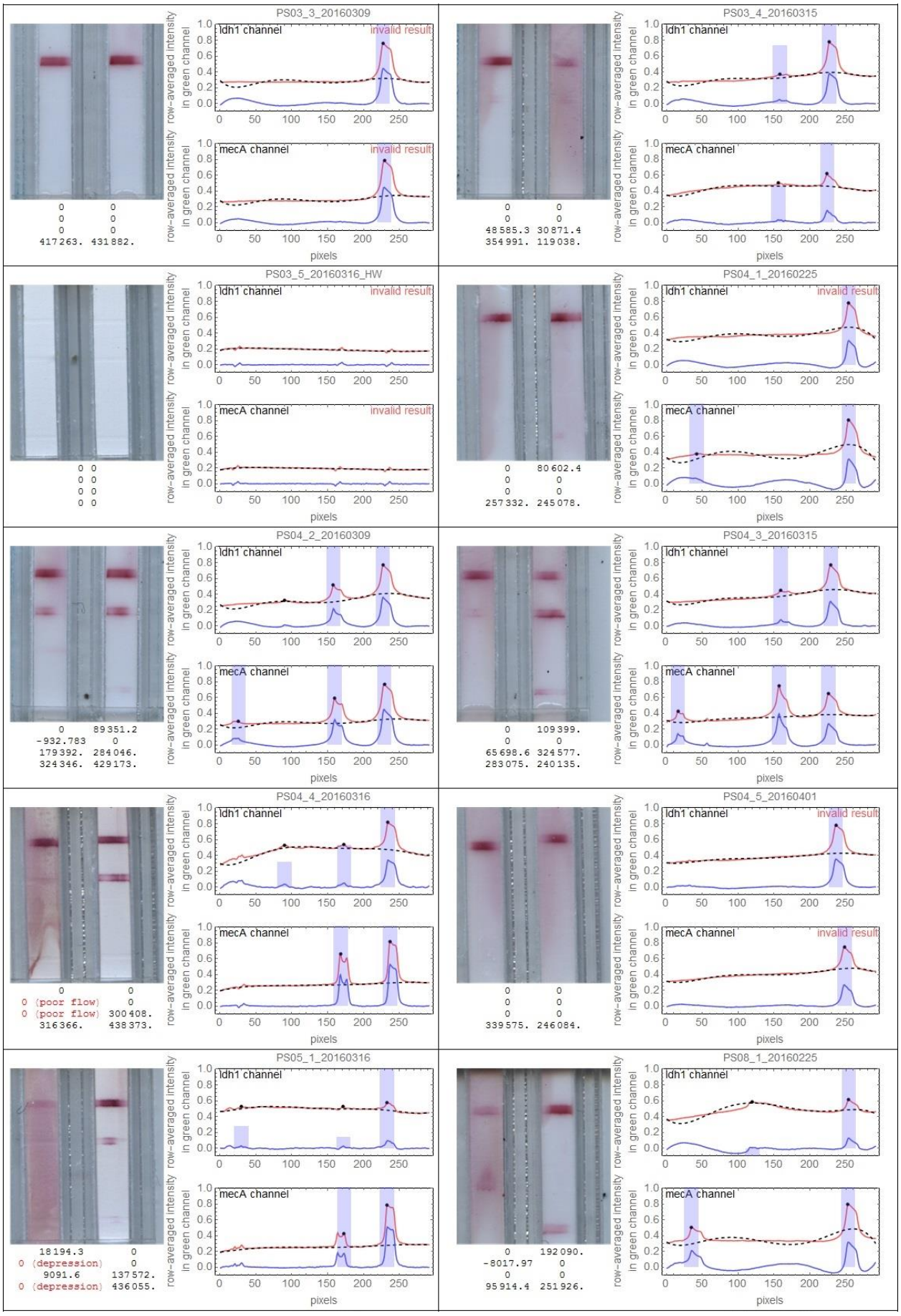
PS03_3_20160309
ldh1 channel
invalid result
mecA channel
invalid result
row-averaged intensity in green channel
pixels
0 0
0 0
0 0
417263. 431882.
PS03_4_20160315
ldh1 channel
mecA channel
0 0
0 0
48585.3 30871.4
354991. 119038.
PS03_5_20160316_HW
ldh1 channel
invalid result
mecA channel
invalid result
0 0
0 0
0 0
0 0
PS04_1_20160225
ldh1 channel
invalid result
mecA channel
0 80602.4
0 0
0 0
257332. 245078.
PS04_2_20160309
ldh1 channel
mecA channel
0 89351.2
-932.783 0
179392. 284046.
324346. 429173.
PS04_3_20160315
ldh1 channel
mecA channel
0 109399.
0 0
65698.6 324577.
283075. 240135.
PS04_4_20160316
ldh1 channel
mecA channel
0 0
0 (poor flow) 0
0 (poor flow) 300408.
316366. 438373.
PS04_5_20160401
ldh1 channel
invalid result
mecA channel
invalid result
0 0
0 0
0 0
339575. 246084.
PS05_1_20160316
ldh1 channel
mecA channel
18194.3 0
0 (depression) 0
9091.6 137572.
0 (depression) 436055.
PS08_1_20160225
ldh1 channel
mecA channel
0 192090.
-8017.97 0
0 0
95914.4 251926.

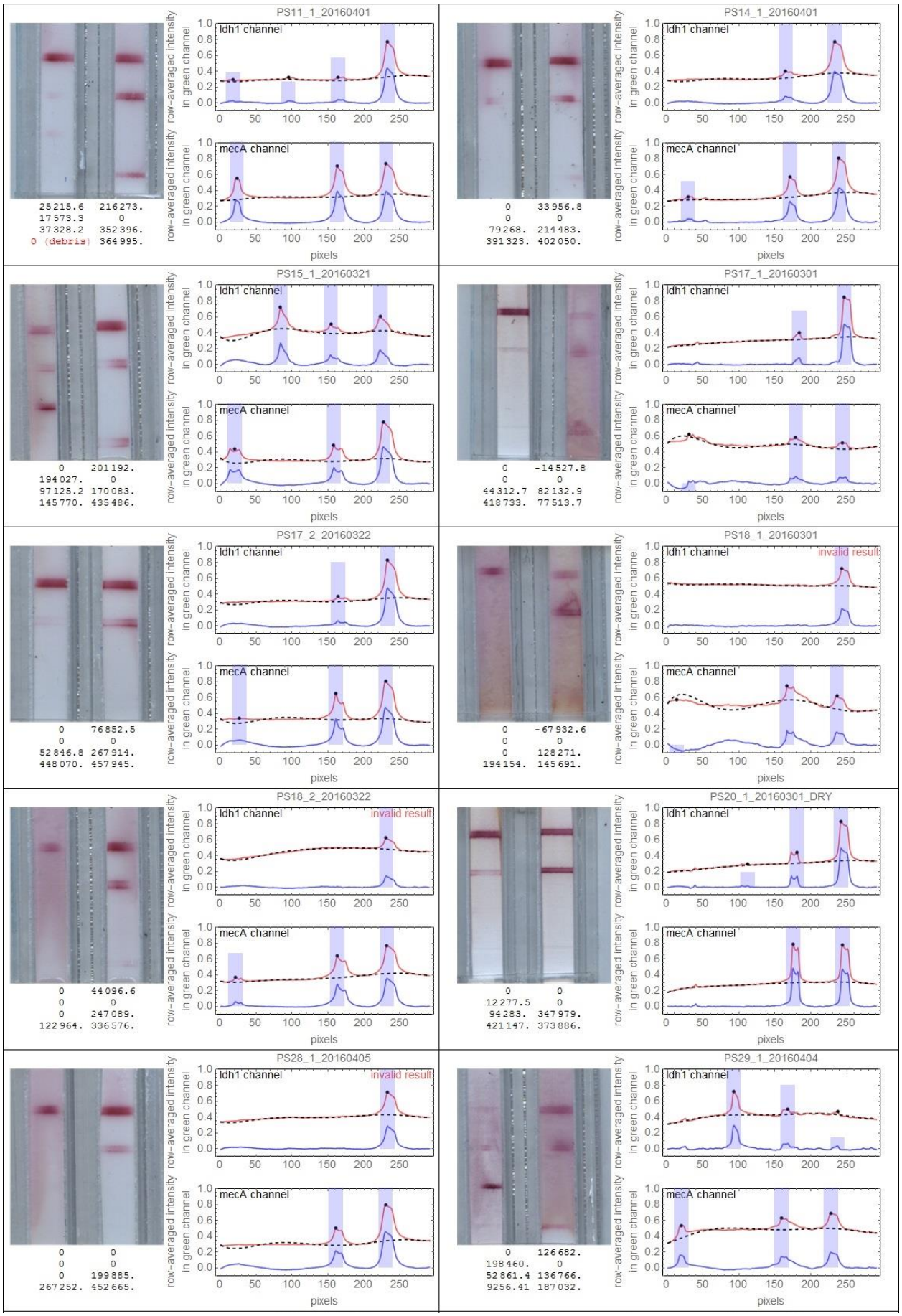
PS11_1_20160401
25215.6 216273.
17573.3 0
37328.2 352396.
0 (debris) 364995.
PS14_1_20160401
0 33956.8
0 0
79268. 214483.
391323. 402050.
PS15_1_20160321
0 201192.
194027. 0
97125.2 170083.
145770. 435486.
PS17_1_20160301
0 -14527.8
0 0
44312.7 82132.9
418733. 77513.7
PS17_2_20160322
0 76852.5
0 0
52846.8 267914.
448070. 457945.
PS18_1_20160301
0 -67932.6
0 0
0 128271.
194154. 145691.
PS18_2_20160322
0 44096.6
0 0
0 247089.
122964. 336576.
PS20_1_20160301_DRY
0 0
12277.5 0
94283. 347979.
421147. 373886.
PS28_1_20160405
0 0
0 0
0 199885.
267252. 452665.
PS29_1_20160404
0 126682.
198460. 0
52861.4 136766.
9256.41 187032.
ldh1 channel
mecA channel
invalid result
row-averaged intensity in green channel
pixels

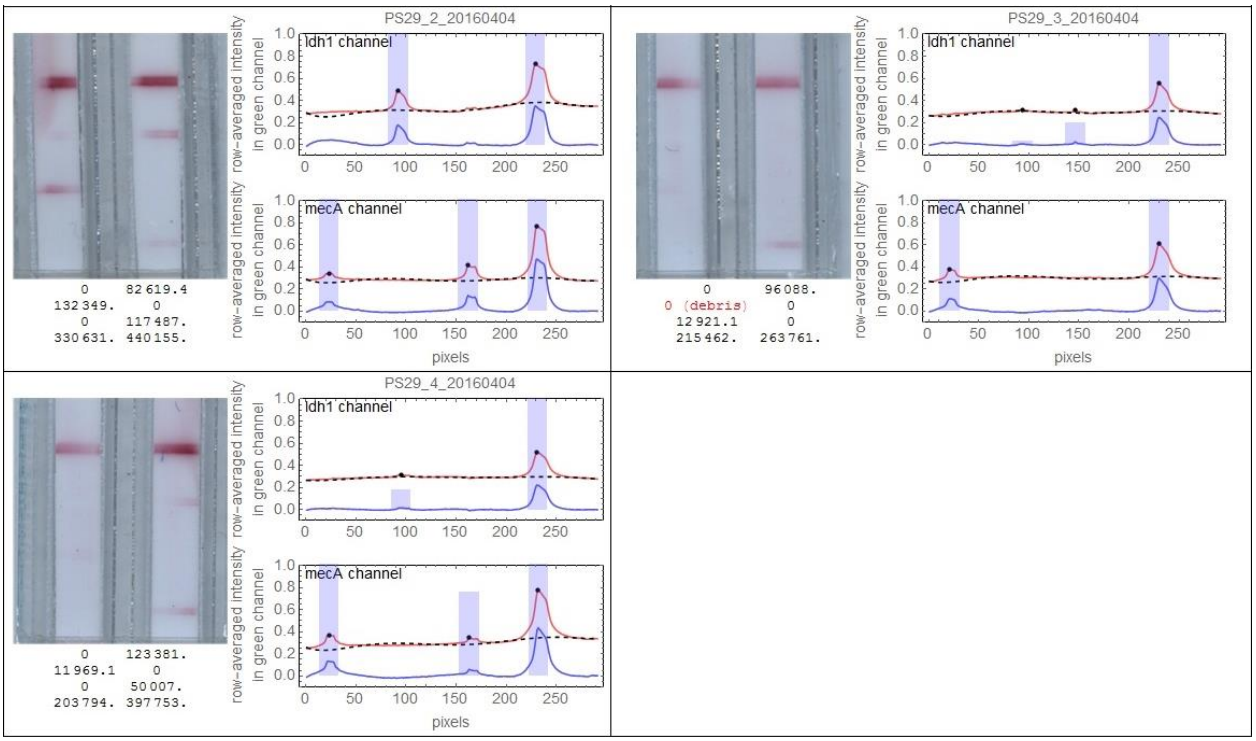


**Fig. S9** LF detection analysis of result images from prototype tests using 33 samples of patient specimens (PS). Test lines were detected as thresholded local maxima (black points) of plot profiles (red lines), which were generated from 50-pixel by 300-pixel regions of the inverted green image channel centered on each LF strip (i.e., *ldh1* and *mecA* channels of each test). Sixth-order polynomials (dashed black lines) were fit to background regions of each plot profile. The background-subtracted plot profiles (blue lines) were integrated within fixed-size regions centered on the local maxima (blue rectangles), with values reported in a table below each image. Occasional poor flow, depressions in the nitrocellulose that were introduced during their manufacture, and debris confounded this algorithm in eight cases, which are marked in red where applicable. Occasional poor flow also contributed to a poor polynomial fit to the background, which resulted in some negative test line intensity values. Invalid results could be due to under heating or overheating (e.g. lysis or amplification was hindered, lysis or amplification valves did not operate properly), or poor flow conditions (e.g. evaporation from uncovered LF strips at a wetting front with high concentration of solute).

**Table S1** Isothermal strand displacement assay (iSDA) nucleic acid sequence designs for primers, probes, and internal amplification control templates.

| | ***ldh1*** | ***mecA*** |
|---|---|---|
| Forward amplification primer (F)<br>(CCTCAGC = nicking site) | 5′–TAG AAT AGT CGC ATA CTT CCTCAGC ACA TCT CCT CGA ACT TTT T–3′ | 5′–CCA TTA TAC TAC CTG TCT CCTCAGC GGC AAA GAT ATT CAA CTA AC–3′ |
| Reverse amplification primer (R)<br>(CCTCAGC = nicking site) | 5′–GCA TAA TAC TAC CAG TCT CCTCAGC CAA GCT ACG CAT TTT CAT T–3′ | 5′–TAG AAT AGT CAC TTA CTT CCTCAGC GCC ATA ATC ATT TTT CAT GTT–3′ |
| Forward bumper primer (FB) | 5′–AGG TAA TGG TGC AGT AGG T–3′ | 5′–GAT AAT AGC AAT ACA ATC GCA CA–3′ |
| Reverse bumper primer (RB) | 5′–CCA GCT TTC ACA CGA AC–3′ | 5′–GTG CTA ATA ATT CAC CTG TTT GA–3′ |
| Capture probe<br>(*pDNA[…]* = pyranosyl DNA) | 4′–*pDNA*[TTTTTTTTC]–2′–HEG–5′–CAG TGT CTA AAT CAA TGA TG–hexanol–3′ | 4′–*pDNA*[CAAGAATC]–2′–HEG–5′–CTT TAG CAT CAA TAG TTA G–hexanol–3′ |
| Biotin probe<br>(A* = Super A®, ElitechGroup) | 5′–CTA ATT CAT CAA CAA TGC–biotin TEG–3′ | 5′–GTT A*TA AAT A*CT CTT TTG A–biotin TEG–3′ |
| Internal amplification control (IAC)<br>(dsDNA template) | 5′–AGG TAA TGG TGC AGT AGG TTC AAG CTA CGC ATT TTC ATT GAC CAG TTA CTT TAC GGA CCA CGT ACC GCA TTG GTA CAA GAT CTC AAA AAG TTC GAG GAG ATG TTG TTC GTG TGA AAG CTG G–3′ | 5′–GAT AAT AGC AAT ACA ATC GCA CAT GGC AAA GAT ATT CAA CTA ACG ACC AGT TAC TTT ACG GAC CAC GTA CCG CAT TGG TAC AAG ATC TCC AAC ATG AAA AAT GAT TAT GGC TTC AAA CAG GTG AAT TAT TAG CAC–3′ |

**Table S2** Genomic copy numbers per mL of *S. aureus* (*ldh1*), methicillin-resistance (*mecA*), *S. epidermidis*, and *S. pyogenes* in samples (1:100 dilution in 10 mM Tris, pH 8.0) of patient specimens calculated from results of separate qPCR assays performed on 1 µL each of samples immediately after ACP lysis of each sample.

| | ***ldh1* qPCR (genomic copies/mL)** | ***mecA* qPCR (genomic copies/mL)** | ***S. epidermidis* qPCR (genomic copies/mL)** | ***S. pyogenes* qPCR (genomic copies/mL)** |
|---|---|---|---|---|
| **PS 3** | ND | ND | $5.80\times10^{6}$ | ND |
| **PS 2** | ND / ND / $1.39\times10^{4}$ | ND / $4.05\times10^{3}$ / $1.21\times10^{4}$ | $1.06\times10^{7}$ | ND |
| **PS 4** | ND / ND | $1.61\times10^{4}$ / $6.73\times10^{4}$ | $8.19\times10^{6}$ | ND |
| **PS 20** | $7.95\times10^{4}$ / ND / $3.00\times10^{4}$ | $7.4\times10^{4}$ / ND / ND | $5.69\times10^{6}$ | ND |
| **PS 17** | ND | $2.69\times10^{4}$ | $5.01\times10^{6}$ | ND |
| **PS 14** | $1.32\times10^{4}$ | $8.45\times10^{5}$ | $8.73\times10^{6}$ | ND |
| **PS 8** | $4.11\times10^{6}$ | $3.99\times10^{4}$ | $1.08\times10^{7}$ | ND |
| **PS 1** | $3.11\times10^{6}$ | $3.17\times10^{6}$ | $8.73\times10^{6}$ | ND |
| **PS 11** | $2.45\times10^{6}$ | $2.36\times10^{6}$ | $6.93\times10^{6}$ | $2.89\times10^{5}$ |
| **PS 29** | $9.78\times10^{6}$ | $8.39\times10^{6}$ | $6.88\times10^{6}$ | ND |
| **PS 15** | $1.35\times10^{7}$ | $1.11\times10^{7}$ | $6.80\times10^{6}$ | ND |